*Int. J. Electrochem. Sci.*, 14 **(2019)** 481 – 493, doi: 10.20964/2019.01.42

International Journal of
ELECTROCHEMICAL
SCIENCE
www.electrochemsci.org

# Direct Fabrication of 3D Graphene–Multi Walled Carbon Nanotubes Network and Its Application for Sensitive Electrochemical Determination of Hyperin

*Lijie Wang*[1,2], *Wenke Jia*[2], *Yanju Wu*[2], *Fei Wang*[2,*], *Lu Kui*[3,*]

[1] College of Chemistry and Molecular Engineering, Zhengzhou University, Zhengzhou, 450001, P R China
[2] School of Material and Chemistry Engineering, Henan University of Engineering, Zhengzhou, 450007, P R China
[3] School of Chemical Engineering and Food Science, Zhengzhou Institute of Technology, Zhengzhou, 450044, P R China
[*]E-mail: wf2003@haue.edu.cn, luckluke@haue.edu.cn

*Received:* 5 September 2018 / *Accepted:* 20 October 2018 / *Published:* 30 November 2018

In this work, pulse potential method (PPM) was proposed to fabricate directly three dimensional graphene (3DG)-multi walled carbon nanotubes (MWCNTs) (3DG-MWCNTs) network on the surface of glassy carbon (GC) electrode in the graphene oxide (GO)-multi walled carbon nanotubes (MWCNTs) (GO-MWCNTs) suspension. GO-MWCNTs and 3DG-MWCNTs were characterized by using scanning electron microscopy (SEM), UV-visible spectrophotometry (UV-vis) and electrochemical experiments. The 3DG-MWCNTs network as a voltammetric material was presented in developing a novel electrochemical sensor for determination of hyperin. Systematic electrochemical tests confirmed that the 3DG-MWCNTs network modified electrode can effectively increase the response to the redox of hyperin, compared with that of bare GC electrode and 3DG network modified electrode. Under the optimal conditions, the response of the sensor demonstrated a linear relationship with hyperin concentration in the range of $5.0 \times 10^{-9} \sim 1.5 \times 10^{-6}$ mol $L^{-1}$ with a low detection limit of $1.0 \times 10^{-9}$ mol $L^{-1}$. Moreover, the proposed method showed excellent performance in stability, sensitivity, selectivity and reproducibility for the determination of hyperin.

**Keywords:** pulse potentiostatic method, 3D graphene, voltammetric sensor, graphene-multi walle

## 1. INTRODUCTION

Hyperin (quercetin 3-D-galactoside), as an important natural ingredient, is awfully common in many plants like clusiaceae , rosaceae and anemone [1]. It is extracted from either Hyperin perforatum L. or the leaves of Zanthoxylum bungeanum via solvent extraction, column chromatography, and

crystallization [2]. Hyperin have been widely used in traditional Chinese medicine due to many pharmacological activities [3]. It not only can be used as anti-inflammatory [4] and antioxidants [5,6], but also as anti-depressant [7]. In addition, hyperin also showed good protective effect on myocardial ischemia reperfusion and cerebral infarction. From the perspective of pharmacological activity and clinical application, it is necessary to establish a sensitive and simple method for determination of hyperin concentration.

Up to now, some kinds of analytical approaches have been proposed for the determination of hyperin, such as high performance liquid chromatography (HPLC) [8-10], reverse phase high performance liquid chromatography (RP-HPLC) [11] and capillary electrophoresis (CE) [12-14]. Although these methods offer commendable accuracy and sensitivity, they require complex and time-consuming experimental procedure, expensive and complicated apparatus. Comparing with these methods, electrochemical methods have some advantages in the analysis of electroactive molecules to make up for this deficiency, such as the accuracy, sensitivity, simplicity, real-time detection, lower cost easy handling and ease of on-site applications and so on. Especially, electrochemical techniques provide critical superiority consists in the redox mechanism and pharmacological action. In the case of hyperin, different electrochemical approaches have been reported, for example, carboxylic multiwalled carbon nanotube (c-MWCNT) modified composite pencil graphite (CPG) electrode via electrophoretic deposition (EPD) [15], poly(3,4-ethylenedioxythiophene)/β-cyclodextrin (PEDOT/β-CD) [16] and poly (diallydimethylammonium chloride)–functionalized graphene modified GC electrode (PDDA-Gr/GCE) [17] have been designed for determination of hyperin.

Graphene (as a two-dimensional (2D) carbon material) has been widely applied in electrochemical sensor due to its unusual electrical conductivity, large specific surface and excellent electrochemical stability [18]. Ever since its introduction in 2004 [19,20], these properties of graphene make them extremely attractive in the field of electronic devices [21], energy conversion and storage devices [22], sensors and biosensors [23]. Chemical reduction of exfoliated graphene oxide (GO) was an efficient approach to preparing graphene. However, easy aggregation in aqueous solution and hydrophobicity of graphene sheets that inevitably occur due to the strong π-π interactions results in the loss of effective surface area [24]. To avoid this problem, it is very important and interesting to design and fabricate a three-dimensional (3D) graphene (3DG) networks of highly porous structures. These 3DG networks have an extraordinary surface area that allows target analytes to be more easily access to a single graphene sheet [36], and produce a continuous ion transport pathway due to its unique porous structure, which in turn reduces the mass transfer resistance of the electrode. Recently, various methods have been proposed to fabricate 3DG including template method [25], chemical vapor deposition (CVD) method [26], chemical reduction method [27] and electrochemical reduction of GO sheets method [28]. Among these methods, electrochemical reduction method provides several advantages over other graphene fabrication techniques, including being green, efficient, inexpensive, and rapid [33]. More importantly, the method can form a stable film on the electrode surface without any further treatment, and the electrochemically prepared graphene sheets are more conducting than that prepared from other methods [29,30]. Recently, we reported that pulse potential method (PPM) can obtain uniform and wrinkled electrochemically reduced graphene oxide (ErGO), and the ErGO film are almost aligned perpendicularly to the surface of the glassy carbon (GC) electrode [31-32]. Also, it is the most convenient

and effective way for electrode surface modification since it can directly prepare graphene-based nanocomposites form relatively stable GO suspension [33].

In this work, PPM was proposed to directly fabricate three dimensional graphene (3DG)-multi walled carbon nanotubes (MWCNTs) (3DG-MWCNTs) network on the surface of GC electrode. The 3DG-MWCNTs network as a voltammetric material was presented in developing a novel electrochemical sensor for determination of hyperin. The electrochemical behavior of hyperin on the 3DG-MWCNTs network modified GC electrode was investigated by cyclic voltammetry (CV), chronoamperometry (CA) and differential pulse voltammetry (DPV). Under the optimal conditions, the response of the result modified electrode demonstrated a linear relationship with hyperin concentration. In addition, this method was also successfully employed for determination of hyperin in real sample with satisfactory results.

## 2. EXPERIMENTAL

### *2.1. Apparatus and reagents*

Electrochemical experiments were conducted at the RST5000 electrochemical workstation (Zhengzhou Shiruisi Instrument Technology Co., Ltd., Zhengzhou, China) and model CHI 650A electrochemical system (CHI Instrumental, Shanghai, China). Scanning electron microscopic (SEM) images of the prepared 3DG and 3DG-MWCNTs were obtained with a field emission scanning electron microscopic (FESEM) of MERLIN (Zeiss Co., Germany). Atomic force microscopy (AFM) images were acquired on a Dimension FastScan AFM (Bruker Co., Germany). Raman spectra were obtained using an inVia Reflex Raman spectrometer (Renishaw Co., English). The UV-vis absorption spectrum was acquired on a UV-2102 spectrophotometer (Unico Co., China).

Highly pure graphite powder (325 meshs) and multi-wall walled carbon nanotubes (MWCNTs) (OD: 10-20 nm; L: 0.5-2 μm; purity >95%) were purchased from Xfnano Materials Tech Co., Ltd. (Nanjing, China). Hyperin, ethanol (EtOH), potassium ferricyanide, sulfuric acid (98.0%), potassium permanganate, hydrogen peroxide solution (30%), hydrochloric acid (36.0%-38.0%) was purchased from Aladdin Chemistry Co., Ltd. (Shanghai, China). Reagents that involved with experiments were all of analytical grade, without further procedure of purification. Double distilled water (DDW) was used for all preparations.

### *2.2. Preparation of GO-MWCNTs suspension*

The GO sheet was synthesized from natural graphite as starting materials according to the Hummers method [34]. Prepared GO sheet was centrifuged at 4000 rpm to remove the unreacted graphite powder. And then exfoliate GO was produced by ultrasonic treatment for 3 hours. 3 mg $mL^{-1}$ GO suspension was obtained through diluted treatment. Finally, 3 mg MWCNT was added to 10 mL 3 mg $mL^{-1}$ GO suspension, and then ultrasonic treatment was carried out for 30 min to obtain the GO-MWCNTs suspension.

### *2.3. Preparation of 3DG-MWCNTs network modified electrode*

Before modified, the bare glassy carbon electrode (GCE) was polished successively to a mirror on the surface of 0.3 and 0.05 μm alumina slurry and flushed with pure water and subsequently was sonicated in ethanol and DDW each for 1 min. After that, cleaned bare GCE was immersed in GO-MWCNTs suspension, and electrochemical deposition was performed by PPM with constant stirring. The resulted modified electrode was called 3DG-MWCNTs/GCE. The parameters of electrodeposition listed as follows: upper limit potential $E_a$, 0.1 V; cathodic pulse duration $t_c$, 0.7 s; lower limit potential $E_c$, -1.2 V; anodic pulse duration $t_a$, 0.3 s. For a comparison, 3DG/GCE was also fabricated in the same way without adding MWCNTs and only using GO suspension and bare glassy carbon electrode.

## 3. RESULTS AND DISCUSSION

### *3.1. Characterization of GO-MWCNTs suspension*

The inset of Fig. 1 shows the dispersibility of MWCNTs (curve a), GO (curve b) and GO-MWCNTs (curve c) in water. As can be seen in the inset of Fig. 1, MWCNTs show poor dispersion in water due to their high aspect ratio and strong van der waals interactions, as noticed by immediate precipitation of the aggregates of MWCNTs at the bottom of cuvette. When the MWCNTs was added to the the suspension of GO, the change of color from yellow to black is found. The result suggest that MWCNTs may be bonded to GO sheets through the π–π interaction [35]. Further, UV-visible spectroscopy experiments were used to compare the absorption band change of GO and GO-MWCNTs. As seen in Fig. 1, there is almost no absorption of MWCNTs in the range of 200 nm-600 nm. The characteristic absorption of GO and GO-MWCNTs was observed at 240 nm, but the GO-MWCNTs has a significant increase in absorbance. This can be attributed to that MWCNTs can be bonded to GO through the π–π interaction.

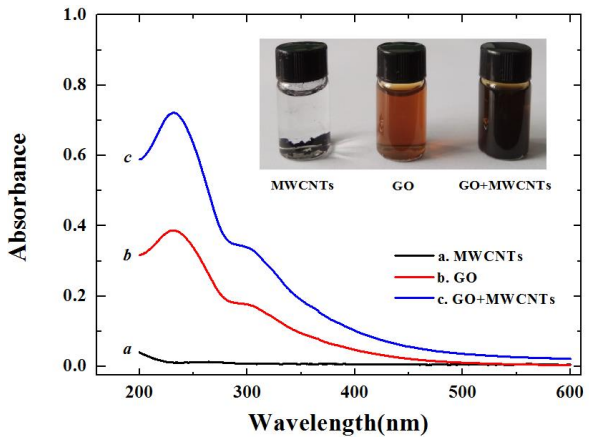


**Figure 1.** UV-visible absorption spectra of MWCNTs (a), GO (b) and GO-MWCNTs (c); the inset shows the photograph of MWCNTs, GO and GO-MWCNTs dispersibility in water.

Furthermore, the morphology of GO and GO-MWCNTs was characterized by AFM. As observed in the AFM image (Fig. 2), many winding attachment on the surface of GO was observed on the AFM

image of GO-MWCNTs, compared with the AFM image of GO sheets. And the average thickness of GO sheets is about 1 nm as measured by the cross-sectional profiles along the lines in the AFM image. But the average thickness of GO-MWCNTs is thicker than GO sheets and increased to about 10 nm. These results further confirmed that MWCNTs was successfully bonded to GO sheets.

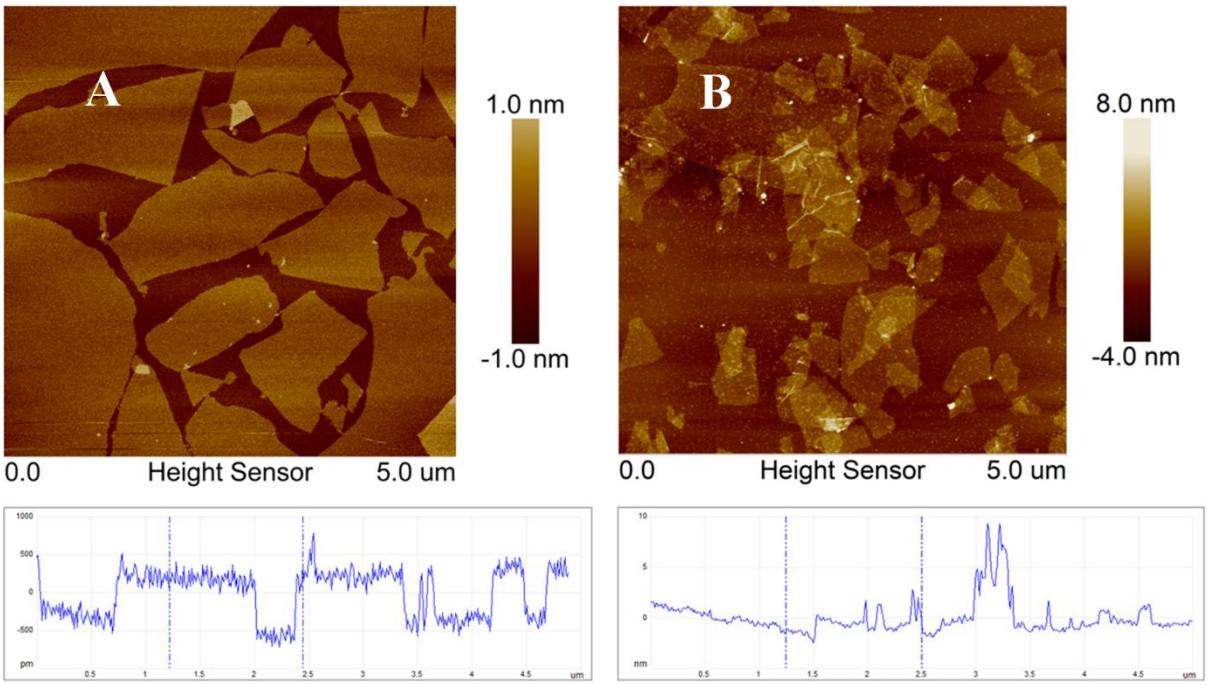


**Figure 2.** AFM image of GO (A) and GO-MWCNTs (B) from their dilute aqueous dispersion on freshly cleaned mica.

*3.2. Characterization of 3DG-MWCNTs network modified electrode*

The scanning electron microscopy (SEM) morphologies of the as-prepared 3DG and 3DG-MWCNTs film in Fig. 3. As can be seen in Fig. 3A-B, a highly porous and interconnected network of 3DG (Fig. 3A) and 3DG-MWCNTs (Fig. 3B) is observed on the electrode surface, respectively. Further, cross-sectional SEM images of 3DG-MWCNTs modified GC electrode was obtained. It is clear that the porous walls consist of upright oriented graphene-MWCNTs sheets (Fig. 3C-D), which can provide a higher active surface and facilitate the access of target analyte to the electrode surface. It is very beneficial for the electrochemical sensing applications. Besides, to this 3DG-MWCNTs network, MWCNTs like a wire connect the graphene sheets and the presence of MWCNTs in graphene-MWCNTs nanocomposites may smooth the "wrinkles" of graphene and prevent further aggregations, which may increase the electron transfer at the interface and help to offer larger specific surface area [36]. Therefore, the electrochemical performance of 3DG and 3DG-MWCNTs modified GC electrodes were directly investigated in the following experiment.

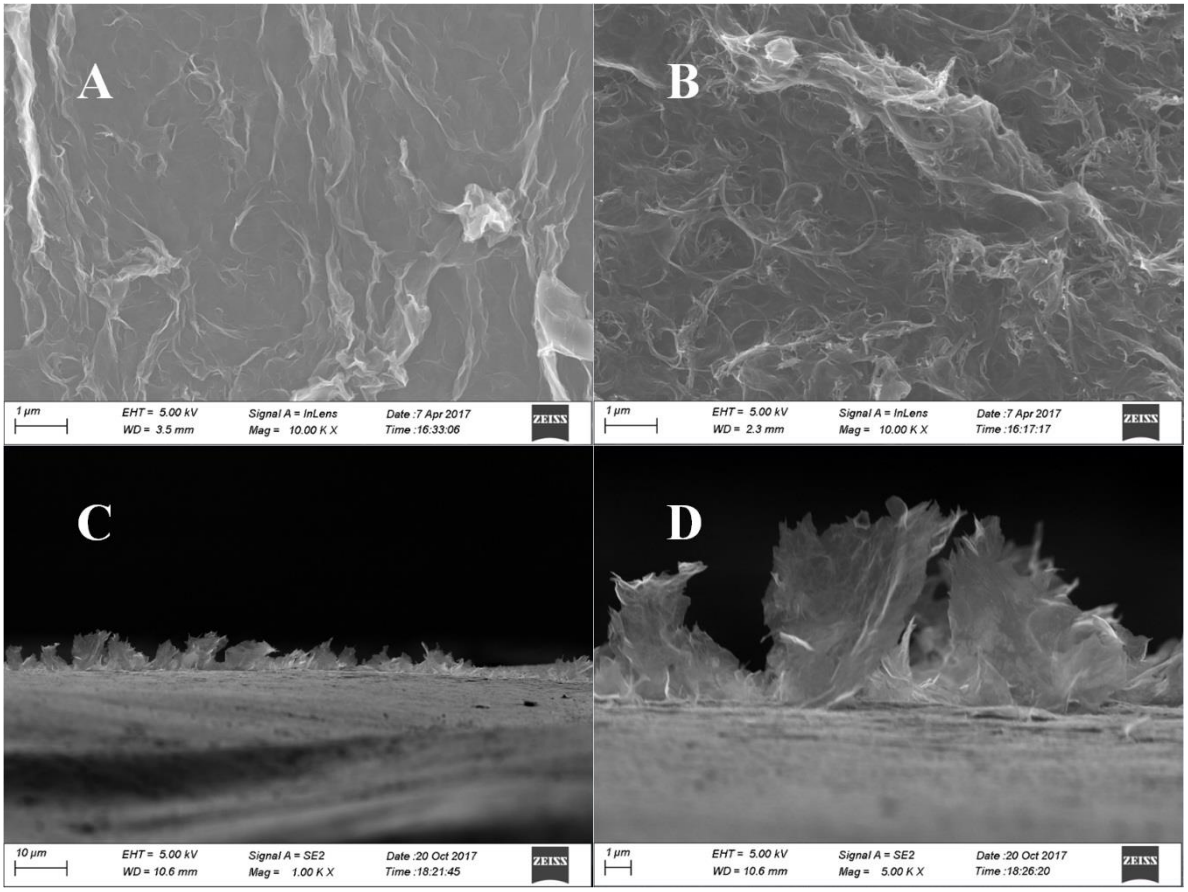


**Figure 3.** Top view SEM images obtained from 3DG/GCE (A) and 3DG-MWCNTs/GCE (B), and different magnification of cross-sectional SEM images obtained from 3DG-MWCNTs/GCE (C and D); (C) 1000 x and (D) 5000 x.

Fig. 4A illustrates the cyclic voltammograms (CVs) curves comparing bare GCE (curve a), 3DG/GCE (curve b) and 3DG-MWCNTs/GCE (curve c) in a $1.0 \times 10^{-3}$ mol $L^{-1}$ $K_3[Fe(CN)_6]$ + 0.1 mol $L^{-1}$ KCl solution at a scan rate of 0.05 V $s^{-1}$. It is found that a pair of redox peak of $[Fe(CN)_6]^{3-/4-}$ on bare GCE with the peak-to-peak separation ($\Delta E_p$) as 91 mV (curve a). Compared with the bare GCE, both anodic and cathodic peak currents ($i_p$) increase significantly with the $\Delta E_p$ value decrease obviously at 3DG/GCE and 3DG-MWCNTs/GCE, which were attributed to the excellent electronic conductivity, respectively. The largest peak currents and the smallest $\Delta E_p$ are observed at 3DG-MWCNTs, indicating that the presence of MWCNTs can increase the electron transfer at the interface and result in a more conductive network. Moreover, based on Randles-Sevcik Equation, the effective surface area of different electrodes can be described as follows [37]: $i_{pa} = 2.69\times10^5 n^{3/2} A D_o^{1/2} c_o v^{1/2}$, where $i_{pa}$ is refers to anodic peak current (A); n is the electron transfer number; $A$ is the surface area of the electrode ($cm^2$); $D_o$ is the diffusion coefficient ($cm^2$); $c_o$ is the concentration of $K_3[Fe(CN)_6]$ (mol $L^{-1}$) and $v$ is the scan rate (V $s^{-1}$). The effective surface areas of bare GCE, 3DG/GCE, 3DG-MWCNTs/GCE were calculated as 0.062, 0.197 and 0.217 $cm^2$, respectively. It confirmed that 3DG and 3DG-MWCNTs network can increase significantly the effective surface area of electrode because of their highly porous properties.

At the same time, the influence of the structure of graphene sheets on electrochemical characterization of modified electrode was also studied using $[Fe(CN)_6]^{3-/4-}$ (Fig. 4B). The 3DG/GCE

and 3DG-MWCNTs/GCE were left to dry in the air. Under this circumstance, the entrapped water inside the network evaporated gradually. The result caused the 3D structure with highly porous to collapse and form a compact 2D layer due to the strong π-π interactions. As a result, the peak currents of the redox probe $[Fe(CN)_6]^{3-/4-}$ decreased dramatically and $\Delta E_p$ increase obviously in its dry state as shown in Fig. 4B. Therefore, the modified GC electrodes must be kept in DDW to prevent the collapse of the porous network when they were not in use.

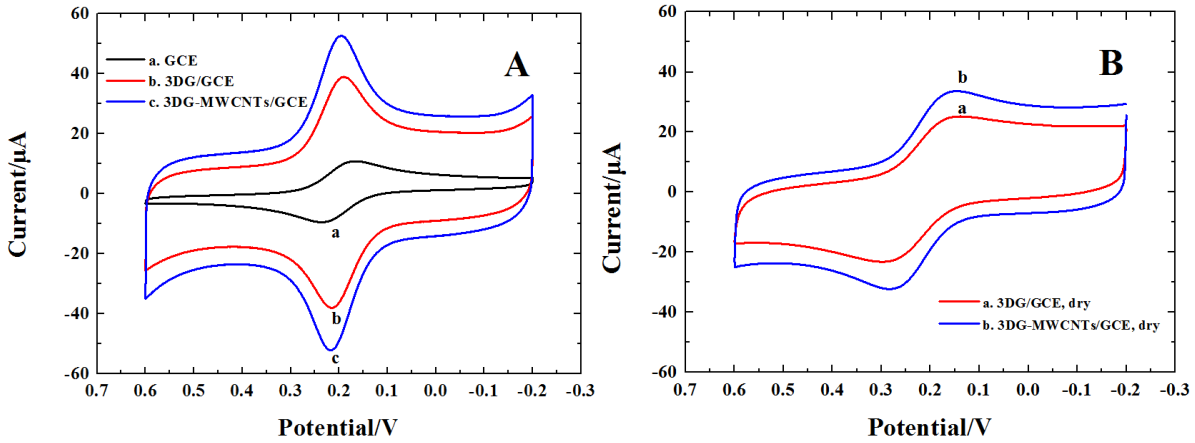


**Figure 4.** (A) CVs of bare GCE (curve a), 3DG/GCE (curve b) and 3DG-MWCNTs/GCE (curve c) in $1.0 \times 10^{-3}$ mol $L^{-1}$ $K_3[Fe(CN)_6]$ + 0.1 mol $L^{-1}$ KCl solution, $v$ = 0.05 V $s^{-1}$; (B) CVs of 3DG-MWCNTs/GCE (curve a) in dry state and 3DG/GCE in dry state (curve b).

### *3.3. Electrochemical behavior of hyperin at 3DG-MWCNTs network modified GC electrode*

The electrochemical behavior of hyperin at different electrodes was investigated by using CV techniques. Fig. 5A shows the CVs of $5.0 \times 10^{-7}$ mol $L^{-1}$ hyperin at bare GCE (curve a), 3DG/GCE (curve b) and 3DG-MWCNTs/GCE (curve c) in 0.1 mol $L^{-1}$ $H_2SO_4$ solutions, respectively. As can be seen, hyperin showed electrochemical activation at all electrodes. At the bare GCE, only a weak and small of redox peak is observed for hyperin. In contrast, the redox peak currents of hyperin increased significantly at the 3DG/GCE. When the 3DG-MWCNTs/GCE was applied, a distinct well-defined and more sensitive redox peaks appeared under the same experimental condition, of which the oxidation peak current is about 45.8- and 3.3- fold higher than that of GCE and 3DG/GCE, respectively, and the $\Delta E_p$ is the lowest. The result indicates that the 3DG-MWCNTs network can provide a more efficient interface for the electrochemical response of hyperin compared with that of bare GCE and 3DG/GCE. It also suggests that the presence of MWCNTs in the 3DG-MWCNTs nanocomposite can improve the conductivity. Therefore, 3DG-MWCNTs modified GC electrode was selected as the electrochemical sensor for investigating the voltammetric behavior of hyperin and establishing the electroanalytical method.

To further evaluate the electrode reaction of hyperin, the influence of scan rates ($v$) on the electrochemical response of hyperin was investigated. Fig. 5B shows CVs of $5.0 \times 10^{-7}$ mol $L^{-1}$ hyperin in the 3DG-MWCNTs/GCE with $v$ ranging from 0.1 to 1.0 V $s^{-1}$. With the increasing of $v$, the oxidation peak current ($i_{pa}$) and reduction peak current ($i_{pc}$) of hyperin grows gradually and the plot of the redox

current ($i_p$) and $v$ shows a good linear relationship, indicating that this is an adsorption-controlled process. Based on Laviron's theory of an absorption-controlled process, the relation of $i_p$ and $v$ can be described as follows [38]: $i_p=nFQv/4RT$. The equation shows that the $n$ can be calculated as long as the $Q$ is obtained. As the scan rates varied from 0.1 to 1.0 V $s^{-1}$, n = 2 was determined as an average. Furthermore, the oxidation peak potentials ($E_{pa}$) shift positively and the reduction peak potentials ($E_{pc}$) shift negatively with the increasing $v$, and good linear relationships are observed between the peak potentials and the napierian logarithm (ln$v$) of the scan rates. From the slope of $E_{pa}$ *vs.* ln$v$ and $E_{pc}$ *vs.* ln$v$ [39], the kinetic parameter $\alpha n$ is calculated to be 0.96. Consequently, the value of $\alpha$ is calculated to be 0.48.

To illustrate further the electrochemical oxidation mechanism of hyperin, the effect of different pH values on the redox of hyperin was also investigated to discuss the number of transferred protons ($m$) (Fig. 5C). The result shows that $E_{pa}$ and $E_{pc}$ shifts negatively with increasing the pH values, and plots between the formal peak potential ($E^{o'}=(E_{pa}+E_{pc})/2$) and pH show a linear relationship. The slope value is -62 mV $pH^{-1}$, which is identical to the theoretical value. The result suggests that the redox of hyperin is the equal number of transferred protons and electrons. Based on the above results, a possible electrochemical reaction mechanism of hyperin can be written as Scheme 1. Moreover, the redox peak current of hyperin reached to its maximum in 0.1 mol $L^{-1}$ $H_2SO_4$ (pH=0.95). Hence, in 0.1 mol $L^{-1}$ $H_2SO_4$ (pH=0.95) was used in the Analytical application.

Catalytic rate constant ($k_{cat}$) of hyperin on the surface of 3DG-MWCNTs modified GC electrode was also studied by CA. Fig. 5D shows chronoamperometric curves of the background (curve a) and 5.0 × $10^{-5}$ mol $L^{-1}$ hyperin (curve b) in 0.1 mol $L^{-1}$ $H_2SO_4$ at the 3DG-MWCNTs/GCE. According to previous report [32], the corresponding $i_{cat}/i_L$ versus $t^{1/2}$ plot is presented and showed as the inset in Fig. 5D. From the slope of the straight line, the $k_{cat}$ is calculated to be 1.74 × $10^3$ mol $L^{-1}$ $s^{-1}$, which is much larger than that of bare GCE (78.9 mol $L^{-1}$ $s^{-1}$) and 3DG/GCE (0.84 × $10^3$ mol $L^{-1}$ $s^{-1}$). The result further suggested that the 3DG-MWCNTs networks film can provide a more efficient interface for the electrochemical response of hyperin.

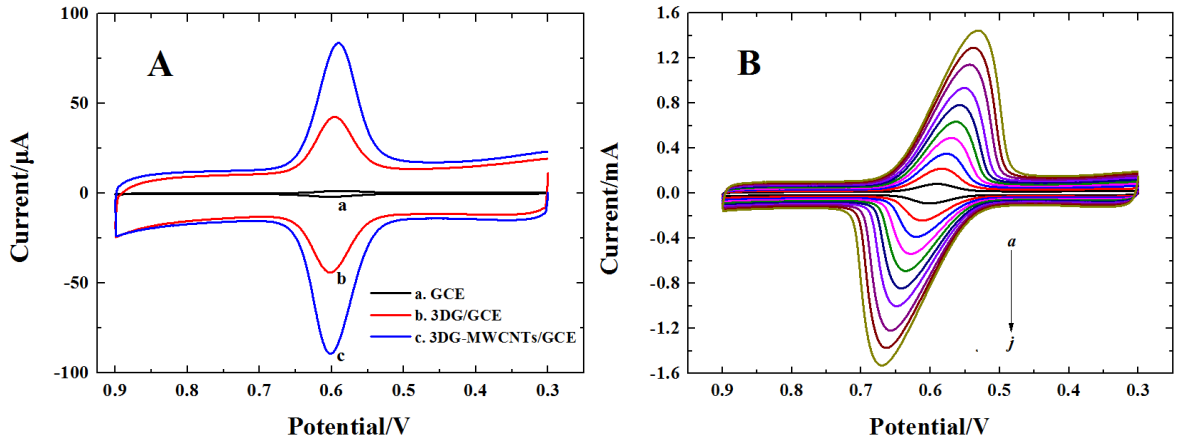

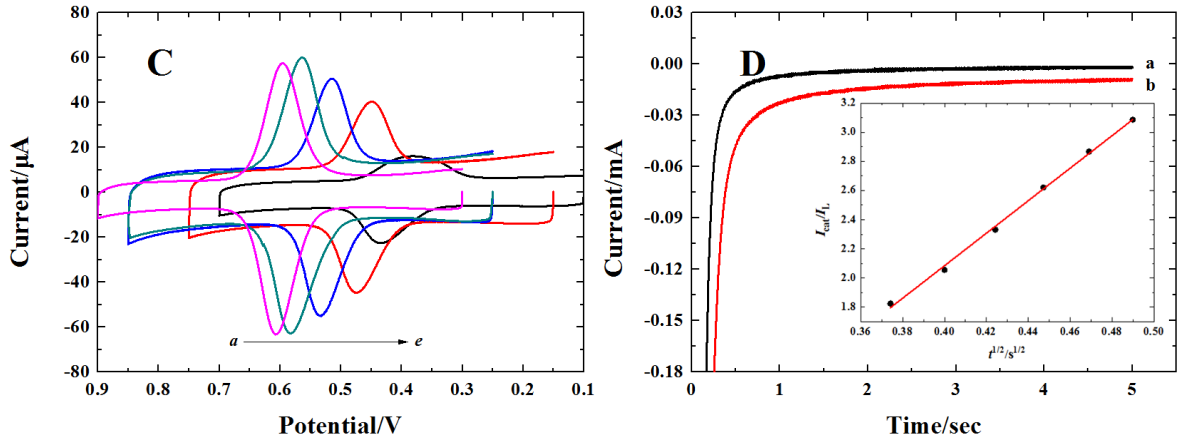


**Figure 5.** (A) CVs of $5.0 \times 10^{-7}$ mol $L^{-1}$ hyperin at a bare GCE (curve a), 3DG/GCE (curve b) and 3DG-MWCNTs/GCE (curve c) in 0.1 mol $L^{-1}$ $H_2SO_4$, $v$ = 0.10 V $s^{-1}$; (B) CVs of $5.0 \times 10^{-7}$ mol $L^{-1}$ hyperin at the 3DG-CMWCNTs/GCE at different scan rate (from *a* to *j*: 0.10, 0.20, 0.30, 0.40, 0.50, 0.60, 0.70, 0.80, 0.90 and 1.00 V $s^{-1}$); (C) CVs of $5.0 \times 10^{-7}$ mol $L^{-1}$ hyperin at the 3DG-MWCNTs/GCE at different pH values, $v$ = 0.05 V $s^{-1}$; (D) Chronoamperometric curves of the background (curve a) and $5.0 \times 10^{-5}$ mol $L^{-1}$ hyperin (curve b) in 0.1 mol $L^{-1}$ $H_2SO_4$ at the 3DG-MWCNTs/GCE; the inset shows the corresponding relationship of $i_{cat}/i_L$ versus $t^{1/2}$.

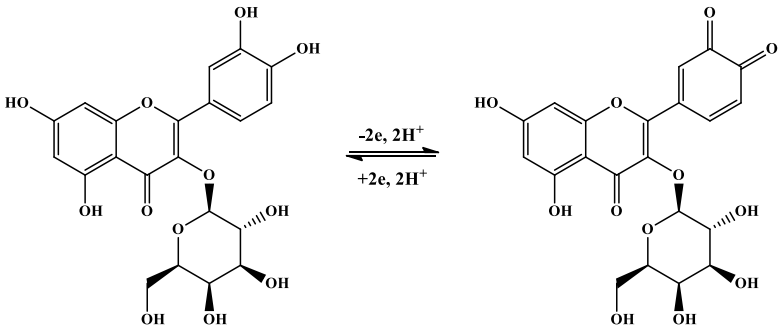


**Scheme 1.** The proposed redox mechanism of hyperin at the 3DG-MWCNTs/GCE.

### *3.4. Analytical application and method validation*

#### *3.4.1. Optimization of parameters for determination of hyperin*

The oxidation peak was chose as the detection signal and DPV was chose as an analytical technique to establish the analytical method for hyperin. The effect of accumulation time ($t_{acc}$) and accumulation potential ($E_{acc}$) on oxidation peak current of hyperin was also studied. The $t_{acc}$ of 240 s under open circuit was used for further studies.

Here renewal of the electrode is achieved upon immersion of the modified GC electrode in 0.1 mol $L^{-1}$ $H_2SO_4$ solution for 5 min under stirring. And CV was then carried out in the potential ranging from 0.3 V to 0.9 V (*vs* SCE) until the redox peaks of hyperin disappeared. The renewed electrode exhibited almost the same characteristics as the initial state, indicating that the performance of 3DG-CMWCNTs network was not damaged.

*3.4.2. Analytical performances*

Under the optimal conditions, the calibration curve for determination of hyperin was established. Fig. 6A shows the superimposed differential pulse voltammetric curves of a series of hyperin concentrations. The currents of response show a linear relationship with hyperin concentration in the range of $5.0 \times 10^{-9} \sim 1.5 \times 10^{-6}$ mol $L^{-1}$. The linear regression equation and correlation coefficient as follows:

$i_{pa}$ (μA) = 12.87 + 372.6*c* (μmol $L^{-1}$) (R=0.995)

The limit of detection (LOD) of $1.0 \times 10^{-9}$ mol $L^{-1}$ is calculated by signal-to-noise ratio of 3 (S/N) [40]. Table 1 shows the analytical method and analytical properties of several hyperin biosensors found in the literature [15-17]. As it can be observed, It is obvious that the proposed method showed a wider linear ranges and lower detection limits. The results suggested that the 3DG-MWCNTs network fabricated by PPM can be used satisfactorily as electrochemical sensor materials.

The reproducibility of the electrode fabricated for sensing of hyperin was further investigated, expressed in terms of relative standard deviation 3.7% at a hyperin concentration of $5.0 \times 10^{-7}$ mol $L^{-1}$ was obtained, which showed high reproducibility of the 3DG-MWCNTs for hyperin detection. To characterize stability, after storage at 4°C for 2 weeks, it was observed that a loss of 5.2% of the initial peak current was remained. The results indicate that the biosensor has good stability.

**Table 1.** Comparison of determination of hyperin by different methods of electrochemical sensor reported

| Electrode | Methods | Linear range (mol $L^{-1}$) | Detection limit (mol $L^{-1}$) | Reference |
|---|---|---|---|---|
| c-MWCNT/CPGE | DPV | $2.2\times10^{-7} \sim 1.0\times10^{-5}$ | $1.0 \times 10^{-7}$ | [15] |
| PEDOT/β-CD/GCE | DPV | $7.0\times10^{-9} \sim 5.0\times10^{-6}$ | $2.3\times10^{-9}$ | [16] |
| PDDA-rGO/GCE | DPASV | $7.0\times10^{-9} \sim 2.0\times10^{-7}$ | $5.0\times10^{-9}$ | [17] |
| 3DG-MWCNTs/GCE | DPV | $5.0\times10^{-9} \sim 1.5\times10^{-6}$ | $1.0\times10^{-9}$ | This work |

DPASV: differential pulse adsorptive stripping voltammetry

*3.4.3. Interference studies*

Potential interferences of nature products, some flavonol (including diosmin, quercetin, hesperetin and rutin), dopamine, food accessories (including glucose) and common food preservatives (including ascorbic acid) coexisting with hypeirn were investigated, we compared the electrochemical response toward $1.0 \times 10^{-6}$ mol $L^{-1}$ hyperin before and after 10-fold amounts of interfering compounds (Fig. 6B). It was observed that the electrochemical response did not change significantly (signal change below 5%). Moreover, it was also found that $Ca^{2+}$, $Zn^{2+}$, $Mg^{2+}$, $Cu^{2+}$ and $Fe^{2+}$ in 100-fold of hyperin had

almost no influence with the determination hyperin. All these results indicated the electrochemical sensor has excellent selectivity toward hyperin.

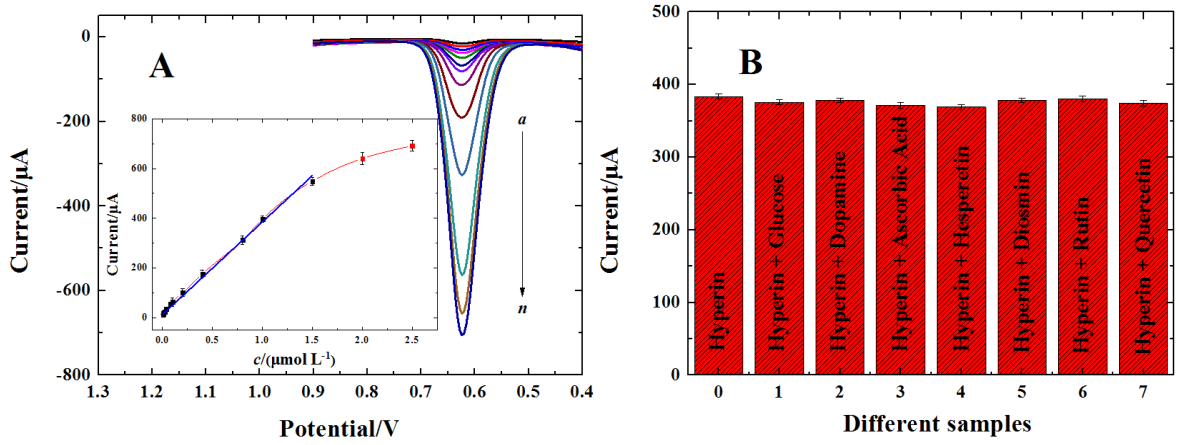


**Figure 6.** (A) DPVs of 3DG-MWCNTs/GCE in 0.1 mol $L^{-1}$ $H_2SO_4$ containing different concentrations of hyperin under optimum conditions, hyperin concentration: (a) $5.0 \times 10^{-9}$ mol $L^{-1}$, (b) $8.0 \times 10^{-9}$ mol $L^{-1}$, (c) $1.0 \times 10^{-8}$ mol $L^{-1}$, (d) $2.0 \times 10^{-8}$ mol $L^{-1}$, (e) $4.0 \times 10^{-8}$ mol $L^{-1}$, (f) $8.0 \times 10^{-8}$ mol $L^{-1}$, (g) $1.0 \times 10^{-7}$ mol $L^{-1}$, (h) $2.0 \times 10^{-7}$ mol $L^{-1}$, (i) $4.0\times 10^{-7}$ mol $L^{-1}$, (j) $8.0 \times 10^{-7}$ mol $L^{-1}$, (k) $1.0 \times 10^{-6}$ mol $L^{-1}$, (l) $1.5 \times 10^{-6}$ mol $L^{-1}$, (m) $2.0 \times 10^{-6}$ mol $L^{-1}$, (n) $2.5 \times 10^{-6}$ mol $L^{-1}$; (B) Influence of different interfering compounds on the $i_{pa}$ detected at the 3DG-MWCNTs/GCE.

**Table 2.** Determination results of hyperin in real samples by DPV and HPLC

| | DPV (n=3)[a] | | | | | HPLC | |
|---|---|---|---|---|---|---|---|
| Samples | Amount found (μmol $L^{-1}$) | Standard added (μmol $L^{-1}$) | Total found (μmol $L^{-1}$) | RSD (%) | Recovery (%) | Total found (μmol $L^{-1}$) | RSD (%) |
| Abelmoschus manihot | 0.245 | 0.200 | 0.450 | 2.9 | 104.2 | 0.239 | 1.7 |
| | | 0.500 | 0.733 | 3.8 | 97.1 | | |
| | | 0.800 | 1.035 | 3.2 | 97.9 | | |

a. Average of three determinations

### *3.5. Determination of hyperin in real samples*

To validate the practical application of this method, it was employed to determine the concentration of hyperin in an actual sample (Abelmoschus and Manihot). All the samples were determined for three times under the same conditions, and the results are listed in Table 2. The values of recovery are also calculated to be over the range from 97.1% to 104.2%, suggesting that this method is reliable and has promising application. Moreover, for testing the accuracy of the proposed method, the same sample was compared to those using HPLC method and the result was also listed in Table 2. It is clear that there is no significant difference between them, which indicate that the method is reliable for the quantitative determination of hyperin in Abelmoschus manihot.

## 4. CONCLUSIONS

In this work, 3DG-MWCNTs network was fabricated on the surface of GC electrode by PPM. Take the advantages of as-prepared nanocomposites including larger accessible surface area as well as higher conductivity by bond of MWCNTs to the 3D network. The 3DG-CMWCNTs network was applied as a new voltammetric material for the fabrication of electrochemical platform for determination of hyperin, which showed wider linear range and low detection limit. Moreover, high sensitivity and good selectivity make it very suitable for determination of hyperin concentration in Abelmoschus manihot.

ACKNOWLEDGMENTS
The authors would like to thank the financial sponsored by program for science & technology innovation talents in Universities of Henan Province (No. 16HASTIT002), the National Science Foundation of China (No. 21572046), and key scientific research projects in Universities of Henan Province (No. 16A150029).

## References

1. S. Li, S. Lei, Q. Yu, L. Zou, and B. Ye, *Talanta*, 185 (2018) 453.
2. J. Pei, A. Chen, L. Zhao, F. Cao, G. Ding, W. Xiao, *J Agric Food Chem.*, 65 (2017) 6042.
3. L. Wu, J. Xu, L. Lu, T. Yang, and Y. Gao, *Colloids Surf. A: Physicochem. and Eng. Aspects*, 482 (2015) 203.
4. K. Su-Jin, U. Jae-Young, L. Ju-Young, *Am. J. Chin. Med*, 39 (2011) 171.
5. W. B. Zeng, H. Yu, F. Ge, J. Y. Yang, Z. H. Chen, Y. B. Wang, Y. D. Dai, and A. Adams, *Molecules*, 19 (2014) 6123.
6. Y. Diñeiro García, B. S. Valles, A. Picinelli Lobo, *Food Chem.*, 117 (2009) 731.
7. J. S. Haas, E. D. Stolz, A. H. Betti, A. C. Stein, J. Schripsema, G. L. Poser, S. M. Rates, *Planta Med.*, 77 (2011) 334.
8. R. Liu, J. Zhang, M. Liang, W. Zhang, S. Yan, M. Lin, *J. Pharm. Biomed. Anal.*, 43 (2007) 1007.
9. P. Xue, Y. Zhao, B. Wang, H. Liang, *J. Chromatogr. Sci.* 45 (2007) 216.
10. H. C. Li, K. Sheng, Z. K. Xie, L, Zou, B. X. Ye, *J. Electroanal. Chem.*, 776 (2016) 105.
11. X. Lin, Y. Wang, X. Liu, S. Huang, Q. Zeng, *Analyst*, 137 (2012) 4076.
12. X. J. Zhou, J. Chen, Y. D. Li, L. Jing, Y. P. Shi, *J. Chromatogr. Sci.*, 10 (2015) 1786.
13. C. H. Geng, M. Lin, W. Y. Wang, J. N. Ye, *J. Anal. Chem.*, 63 (2008) 75.
14. Y. Liu, W. J. Li, X. M. Ling, Y. Z. Li, Q. Y. Zhang,Y. Y. Zhao, *Chromatographia*, 67 (2008) 819.
15. Q. G. Zhu, A. N. A. Sujari, S. Ab Ghani, *J. Solid State Electrochem.* 16 (2012) 3179.
16. L. P. Wu, J. K. Xu, L. M. Lu, T. T. Yang, Y. S. Gao, *Colloids Surf. A: Physicochem. and Eng. Aspects*, 482 (2015) 203.
17. H. Li, K. Sheng, Z. Xie, L. Zou, B. Ye, *J. Electroanal. Chem.*, 105 (2016) 776.
18. Y. Wu, H. Song, K. Lu, Y. Ye, M. Lv, Y. Zhao, *Nano*, 12 (2017) 1750087.
19. A. K. Geim, *Science*, 324 (2009) 1530.
20. A. K. Geim, K. S. Novoselov, *Nat. Mater.*, 6 (2007) 183.
21. C. Biswas, Y. H. Lee, *Adv. Funct. Mater.*, 21 (2011) 3806.
22. J. B. Hou, Y. Y. Shao, M. W. Ellis, R. B. Moore, B. L. Yi, *Phys. Chem. Chem. Phys.*, 13 (2011) 15384.
23. Y. Y. Shao, J. Wang, H. Wu, J. Liu, I. A. Aksay, Y. H. Lin, *Electroanal.*, 22 (2010) 1027.
24. J. Yan, T. Wei, B. Shao, F. Q. Ma, Z. J. Fan, M. L. Zhang, C. Zheng, Y. C. Shang, W. Z. Qian, F. Wei, *Carbon*, 48 (2010) 1731.

25. B. G. Choi, M. H. Yang, W. H. Hong, J. W. Choi, Y. S. Huh, *ACS Nano*, 6 (2012) 4020.
26. Z. P. Chen, W. C. Ren, L. B. Gao, B. L. Liu, S. F. Pei, H. M. Cheng, *Nat. Mater.*, 10 (2011) 424.
27. H. Bai, C. Li, X. L. Wang, G. Q. Shi, *J. Phys. Chem. C.*, 115 (2011) 5545.
28. K. W. Chen, L. B. Chen, Y. Q. Chen, H. Bai, L. Li, *J. Mater. Chem.*, 22 (2012) 20968.
29. J. Ping, Y. Wang, Y. Ying, J. Wu, *Anal. Chem.*, 84 (2012) 3473.
30. M. A. Raj, S. A. John, *J. Phys. Chem. C.*, 117 (2013) 4326.
31. F. Wang, Y. Wu, K. Lu, B. Ye, *Sensor. Actuat. B Chem.*, 208 (2015) 188.
32. F. Wang, Y. Wu, K. Lu, L. Gao, B. Ye, *Electrochim. Acta.*, 141 (2014) 82.
33. F. Wang, Y. J. Wu, X. T. Sun, L. Z. Wang, K. Lu, *J. Electroanal. Chem., 824*(2018) 83.
34. W. S. Hummers, R. E. Offeman, *J. Amer. Chem. Soc.*, 80 (1958) 1339.
35. V. Mani, S. M. Chen, B. S. Lou, *Int. J. Electrochem. Sci.*, 8 (2013) 11641.
36. X. P. Yang, Y. Xiang, Y. Heng, F. Wang, *J. Electroanal. Chem.*, 816 (2018) 54.
37. A. J. Bard, L. R. Faulkner, *J. Chem. Educ.*, 60 (2001) 669.
38. M. Sharp, M. Petersson, K. Edström, *J. Electroanal. Chem.*, 95 (1979) 123.
39. E. Laviron, *J. Electroanal. Chem.*, 101 (1979) 19.
40. J. N. Miller, J. C. Miller, Statistics and Chemometrics for Analytical Chemistry, fourth ed, Pearson Education Limited, (2000) 498.